Estimation of intraoperative brain shift by combination of stereovision and doppler ultrasound: phantom and animal model study

Amrollah Mohammadi, Alireza Ahmadian, Amir Darbandi Azar, Ahmad Darban Sheykh, Faramarz Amiri & Javad Alirezaie

International Journal of Computer Assisted Radiology and Surgery
A journal for interdisciplinary research, development and applications of image guided diagnosis and therapy

ISSN 1861-6410

Int J CARS
DOI 10.1007/s11548-015-1216-z

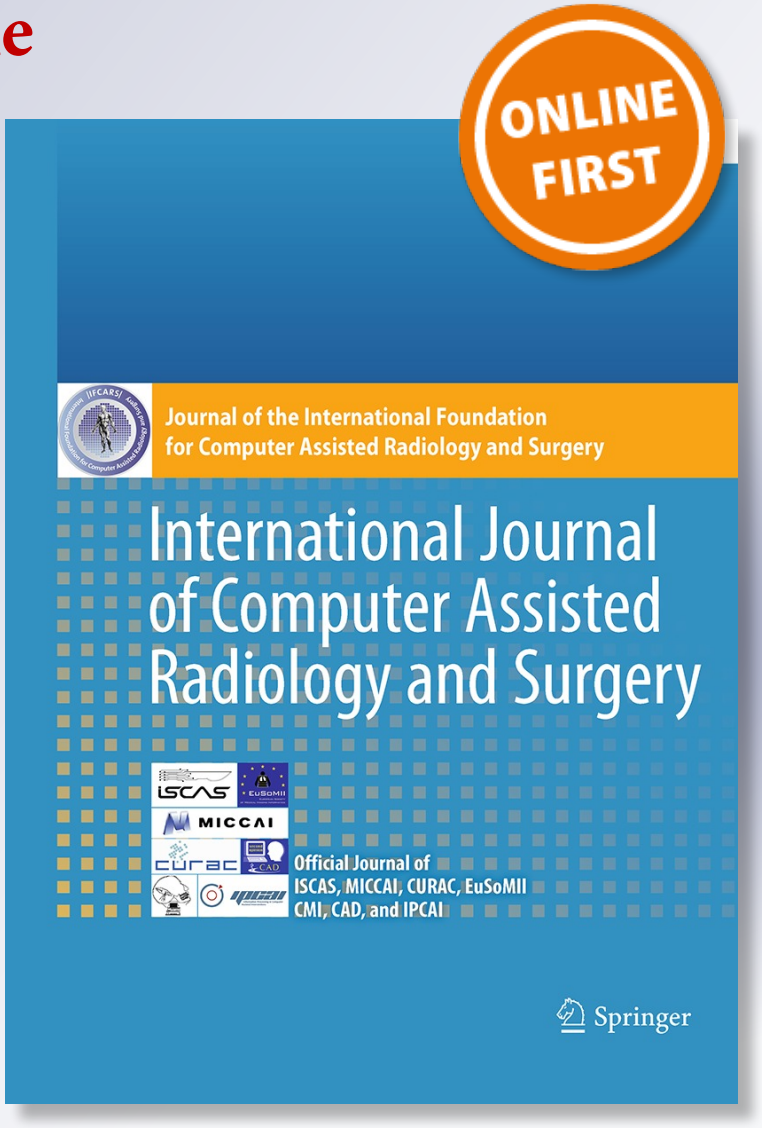

Springer

Int J CARS
DOI 10.1007/s11548-015-1216-z

ORIGINAL ARTICLE

Estimation of intraoperative brain shift by combination of stereovision and doppler ultrasound: phantom and animal model study

Amrollah Mohammadi[1] · Alireza Ahmadian[1] · Amir Darbandi Azar[2] · Ahmad Darban Sheykh[2] · Faramarz Amiri[2] · Javad Alirezaie[3]

Received: 12 January 2015 / Accepted: 21 April 2015

Abstract

Purpose Combination of various intraoperative imaging modalities potentially can reduce error of brain shift estimation during neurosurgical operations. In the present work, a new combination of surface imaging and Doppler US images is proposed to calculate the displacements of cortical surface and deformation of internal vessels in order to estimate the targeted brain shift using a Finite Element Model (FEM). Registration error in each step and the overall performance of the method are evaluated.

Methods The preoperative steps include constructing a FEM from MR images and extracting vascular tree from MR Angiography (MRA). As the first intraoperative step, after the craniotomy and with the dura opened, a designed checkerboard pattern is projected on the cortex surface and projected landmarks are scanned and captured by a stereo camera (Int J Imaging Syst Technol 23(4):294–303, 2013. doi: 10.1002/ima.22064). This 3D point cloud should be registered to boundary nodes of FEM in the region of interest. For this purpose, we developed a new non-rigid registration method, called finite element drift that is more compatible with the underlying nature of deformed object. The presented algorithm outperforms other methods such as coherent point drift when the deformation is local or non-coherent. After registration, the acquired displacement vectors are used as boundary conditions for FE model. As the second step, by tracking a 2D Doppler ultrasound probe swept on the parenchyma, a 3D image of deformed vascular tree is constructed. Elastic registration of this vascular point cloud to the corresponding preoperative data results the second series of displacement vector applicable to closest internal nodes of FEM. After running FE analysis, the displacement of all nodes is calculated. The brain shift is then estimated as displacement of nodes in boundary of a deep target, e.g., a tumor. We used intraoperative MR (iMR) images as the references for measuring the performance of the brain shift estimator. In the present study, two set of tests were performed using: (a) a deformable brain phantom with surface data and (b) an alive brain of an approximately big dog with surface data and US Doppler images. In our designed phantom, small tubes connected to an inflatable balloon were considered as displaceable targets and in the animal model, the target was modeled by a cyst which was created by an injection.

Results In the phantom study, the registration error for the surface points before FE analysis and for the target points after running FE model were <0.76 and 1.4 mm, respectively. In a real condition of operating room for animal model, the registration error was about 1 mm for the surface, 1.9 mm for the vascular tree and 1.55 mm for the target points.

Conclusions The proposed projected surface imaging in conjunction with the Doppler US data combined in a powerful biomechanical model can result an acceptable performance in calculation of deformation during surgical navigation. However, the projected landmark method is sensitive to ambient light and surface conditions and the Doppler ultrasound suffers from noise and 3D image construction

✉ Alireza Ahmadian
ahmadian@sina.tums.ac.ir

Amir Darbandi Azar
amir.doc60@gmail.com

Javad Alirezaie
javad@ee.ryerson.ca

[1] Department of Biomedical Engineering, School of Medicine, Tehran University of Medical Sciences and Research Centre for Biomedical Technology and Robotics (RCBTR), Tehran, Iran

[2] Rajaei Cardiovascular, Medical and Research Center, Tehran, Iran

[3] Ryerson University, Toronto, ON, Canada

problems, the combination of these two methods applied on a FEM has an eligible performance.

Keywords FED registration method · CPD · Finite Element Model · Projected landmarks · Doppler ultrasound · Target registration error

Introduction

In recent two decades, image-guided surgery systems (IGSS) have been widely used in neurosurgical operations. Improvement in accuracy of surgery is the first result of using these systems but when the skull is opened, the problem called "brain shift" can inversely affect accuracy. Brain movements and deformations are hardly predictable and surgeon should estimate displacements mentally and by his/her experience.

Causes of brain deformations during surgery are usually unknown and may be physical such as dura opening, change in the pressure due to loss of cerebrospinal fluid (CSF) and gravity or physiological such as swelling due to drugs, anesthesia or edema. Relating direction and amount of brain shift to nature of pathology, patient's age, craniotomy location is difficult [2–4].

As shown in all studies, deformation mainly occurs in the direction of gravity. Displacement can be downward due to tissue weight and CSF drainage from ventricular system or upward due to intracranial hypertension which may be a result of tumor growth. Deformations are measured using cortical landmarks or tumor region. The amplitudes reported are widely variable from 15 to 24 mm for cortical displacements [2,4] and 8–31 mm for tumor regions [5].

In commercial neuro-navigation systems, the complex brain shift problem remains unresolved and usefulness of these systems is limited to first stages of surgery before large craniotomy or surgeries which need only small opening in the skull. One way for correcting brain deformations is using iMR imaging [6–8]. This solution has some limitation such as its high cost and long image acquisition time that limits the number of images which can be acquired during surgery for tracking brain shifts.

In literature, we can find a number of solutions have been proposed to update preoperative images with intraoperative data. Earlier proposed methods were based on warping preoperative images using image-based models. A number of non-rigid registration methods provided to match intraoperative images (mainly MRI) to preoperative ones [9,10]. Recently, biomechanical models of brain have been developed that can calculate volumetric deformations using surface [11] or contours [12] displacements measured in registered images.

Unlike expensive iMR, some cheap solutions have been proposed that use biomechanical models in conjunction with low-cost intraoperative data such as cortical surface recovered from laser-range scanners [13] or ultrasound images [14]. Image-based methods need high-resolution intraoperative images but in these methods, a proper biomechanical model has a key role in the overall performance of system. Also the model requires adequate validation against clinical data.

Another approach which has been developed by some researchers is using Doppler ultrasound to track the vessels when the brain tissue is deformed [15,16]. When the tumor growth leads to creation of new vessels around it [17], Doppler US imaging seems to be useful for tracking tumor margins. Using vessels displacements recovered by intraoperative 3D Doppler US imaging, Reinertsen et al. in [15] tried to apply a physical thin plate spline (TPS) deformation to preoperative images to correct brain shift. Bucki et al. in [16] proposed a Finite Element Model (FEM) that computes volumetric deformation of brain using sparse displacements of vessels acquired from 2D Doppler US as the model loads.

Recently, researchers are more interested in biomechanical models of brain based mainly on FE modeling. It allows considering complex boundary condition of cortex and skull and physical properties of tissue such as stiffness difference between different parts of brain.

In earlier works, due to lack of proper load definitions and high process power requirements that made it a time-consuming method, FEM did not used in operating rooms. By linearization of model and after improvements in processors, some researchers recommend it for real time surgeries. The assumption of linear model is proper until the displacements of brain tissue are small, but in many surgeries such as tumor resections, the deformation is large and it cannot be modeled by linear FEM. More recently, powerful GPU processors make it possible that nonlinear FEMs can be used for estimating brain shift [18]. However, all studies based on FEM are focused on estimating brain deformation after craniotomy, due to disruption of nodes in the model, none of them models the resections. Few studies have been carried out to model disruptions in FEM [19], but their computations are more complex and inapplicable.

In the present work, we have proposed a framework for estimating brain shift by combination of two sets of intraoperative data: (a) cortical surface data recovered from scanning projected landmarks (b) vascular tree images acquired by Doppler US data. Referring to previous works done by author of this paper [1,20], projecting landmarks to visible surface in order to capture a point cloud of surface is an innovative low-cost method that has adequate accuracy for surface registration. Unlike ultrasound images known as noisy data (compared to other modalities) and difficulties of segmentation of anatomic organs, the Doppler US seems to be more

suitable for tracking vessels. The idea of combination of these two different displacement measures into a biomechanical model can significantly increase the overall accuracy of brain shift estimator. We have attempted to examine this idea. Our idea is near reality because in the biomechanical models when the target points are far from observed deformations (as the model input), the outputs of model would be less accurate. If you prepare more sparse inputs from different areas, the accuracy of outputs would be increased.

At first a phantom study and required procedures and algorithms were implemented as a verification approach to evaluate the proposed method before testing on animal model. Because the simulation of detailed brain vasculature and its blood circulation was difficult, the designed phantom was only used for surface data acquisitions. However many procedures such as 3D model construction, initialization of FEM, tuning scanner of projected landmarks and developing non-rigid registration algorithm were performed in this step of study. The registration algorithm named finite element drift (FED) is a new non-rigid point matching method which is based on elastic deformation concept used in finite element analysis theory. The basic idea is to use a Bayesian framework in which one point set presents Gaussian mixture model (GMM) centroids and drifts toward the other point set in a way which maximizes the likelihood of two point sets. The process of point drift is under the constraint of stiffness matrix of deformed object, and the force applied to each point (node) is iteratively updated.

In order to carry on pre-clinical evaluation of the proposed method, an animal study was performed. This step is necessary before applying human experiments. All our experiments on dogs were carried out under European Union regulations; "*Directive 86/609/EEC*" on the protection of animals used for experimental and other scientific purposes. Finally, one dog was elected for head surgery and after doing craniotomy and data acquisition he recovered safely.

In the rest of the paper, we explain methods of processing preoperative images, building FEM, data acquisition, FE analysis and calculating target registration error (TRE) as measure of estimation accuracy. Results obtained for phantom and animal model will be presented in detail.

Methods and materials

Overall procedure

Figure 1 shows the detailed schematic diagram of the overall procedure proposed for the brain shift compensator as a part of a neuro-navigation system. In the present study, we mainly focused on brain shift estimation, and the compensation part is still under study. The preoperative steps consist of capturing MR and MRA images, the segmentation of the brain followed by building FEM by smoothing and volumetric meshing of the brain, and finally, the segmentation of vessels from the collected MRA images. In the operating room,

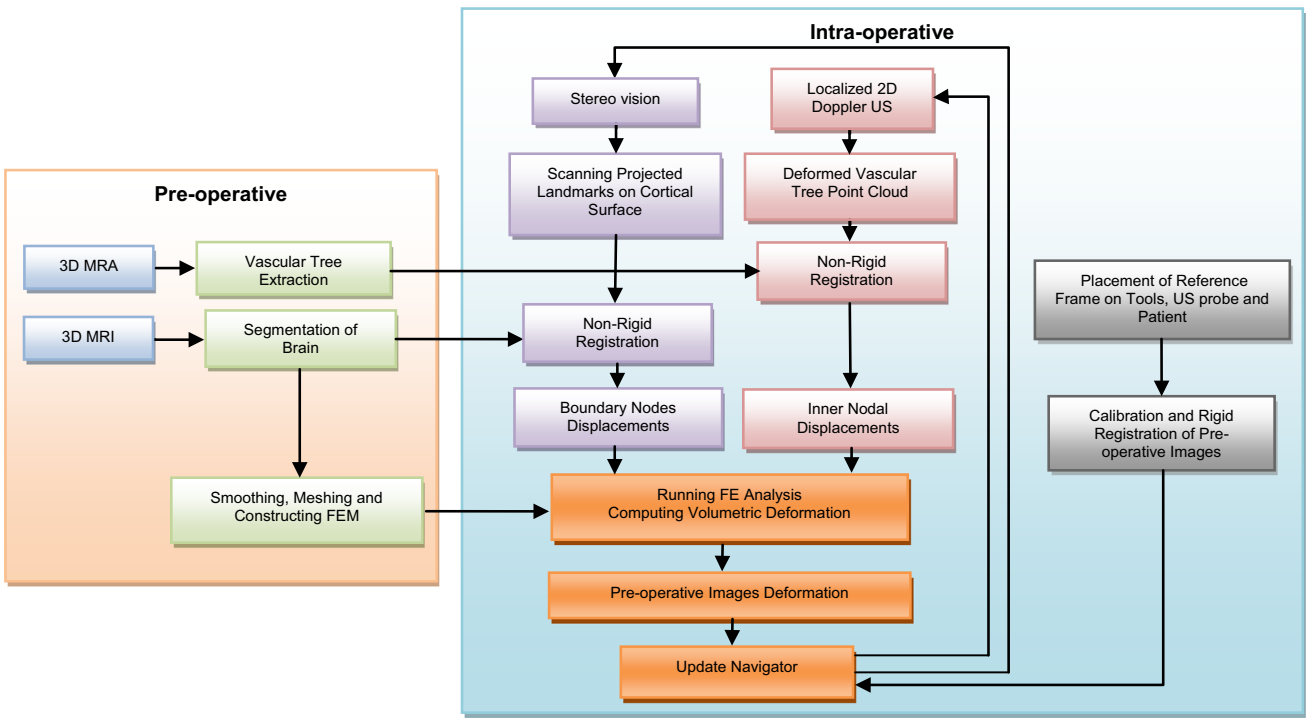

Fig. 1 Schematic diagram of the overall procedure proposed for the brain shift compensator as a part of a neuro-navigation system

after the calibration and rigid registration of the preoperative images, two sets of sparse data were acquired and applied to FEM as external forces to estimate whole brain deformation. The first step involved projecting a designed checkerboard pattern to the visible cortical surface to acquire a 3D point cloud of projected landmarks using a stereo camera. Registering these points to the boundary nodes of FEM yielded the displacement vectors of the cortical surface. The second step involved the acquisition of 2D US Doppler images using a probe that was swept on the parenchyma and tracked by the stereo camera. The 3D point cloud of the segmented vessels from the Doppler images was registered to its preoperative ones to determine sparse vessel displacement vectors. Each vascular displacement vector was assigned to the nearest internal node of FEM. By running FEM with boundary and internal node displacements, the total volumetric deformation was computed, and the displacement of the nodes on the target, e.g., a tumor, can be calculated as the brain shift.

Brain phantom

Constructing a brain phantom is a difficult task when one tries to simulate all details of a real brain. We relied on our previous work that used a phantom in which the brain shift was calculated based on the registration of MRI and US images [21]. The idea of using the elasticity concept as a mechanism for precise and repeatable deformation suitable for MR or CT imaging was used as the minimum required specifications for our study. For Doppler US imaging, a simulated vasculature may be considered, but it was difficult to create small branches of vessels near the cortex using the phantom. Therefore, we decided to use our simple phantom only for surface data acquisition and processing.

Using polyvinyl alcohol cryo-gel (PVAc), a plastic tube, and a balloon that was inflatable to a volume of 10ml, a physical phantom was molded and prepared for testing. Figure 2 shows the prepared phantom and its MR image after inflating to 10 ml. Three series of experiments were performed using an inflation volume of 0, 5, and 10 ml, and MR images and surface scan data were acquired for each case. The MRI apparatus was a SIEMENS Avanto 1.5 T scanner, and a standard T1-weighted scanning sequence at a voxel resolution of $0.78 \times 0.78 \times 0.8$ mm was applied.

FEM of the phantom was built from the MR images that were captured before inflating the internal balloon. The region of interest on the surface of the phantom (where it was more inflated) was manually localized on FEM, and the corresponding boundary nodes were extracted as the first point set. This took almost 220 points. Using the FED method, this point set was registered to the point cloud captured by the stereo camera. The number of captured points was approximately 10 times greater than that of the first point set, thus maximizing the probability of matching the sparse FEM nodes to the corresponding points. To avoid overfitting and to save time, the iterations of the registration algorithm were terminated whenever the total error reduction rate was $<0.1\,\%$. The registration error for each point was defined as the distance between that point and the nearest point in the other point set.

The nodes on the small tubes connected to the balloon were marked as target nodes. After surface registration, the calculated displacement vectors were applied to FEM to compute the displacement of all nodes. Using a rigid-type CPD algorithm, the deformed FEM was registered to the point cloud of the 3D MR images captured after inflating the internal balloon. To evaluate our shift estimator, the TRE was defined as the mean distance between the target nodes and the nearest target points in the post-inflation 3D MR images.

Animal model

A large dog was utilized in the present study. To simulate a target in its brain, the neurosurgeon suggested injecting some water into parenchymal tissue to generate a cyst. The injected water was expected to be absorbed within one day. Prior to craniotomy, a small hole was created on the skull, and approximately 3 ml of water was injected to the parenchymal tissue to create a medium-sized cyst.

After the acquisition of preoperative images, the operation was started. The dog skull was thicker than that of humans; therefore, the neurosurgeon could only open a small bore in it. The visible surface of the cortex was approximately 3×4 cm. Figure 3 shows the dog during the operation and a representative preoperative MR image.

After the acquisition of the proposed intraoperative data, the animal with an opened skull was directed to the MR imaging machine to acquire images that were used for validating our brain shift estimator. The MRI machine and the applied imaging sequences were the same as those mentioned for the phantom.

The initial steps of data analysis for the animal model were similar to that of the phantom, except for a smaller brain volume and cortical surface. Processing of the animal data was performed in three steps. In the first step, only surface displacements were applied to the FE model, and the TRE was computed.TRE was computed using the same method described for the phantom study. Next, we applied only the vessel displacements to the internal nodes of the preoperative FEM. By applying a rigid registration between the surface points of preoperative MRA and the surface nodes of preoperative model, the nearest internal nodes to the vascular points were selected as candidates. After conducting FE analysis, TRE was again computed. For the final step, we combined the surface and vascular data sets of FEM. The results of each step are presented in the Results section.

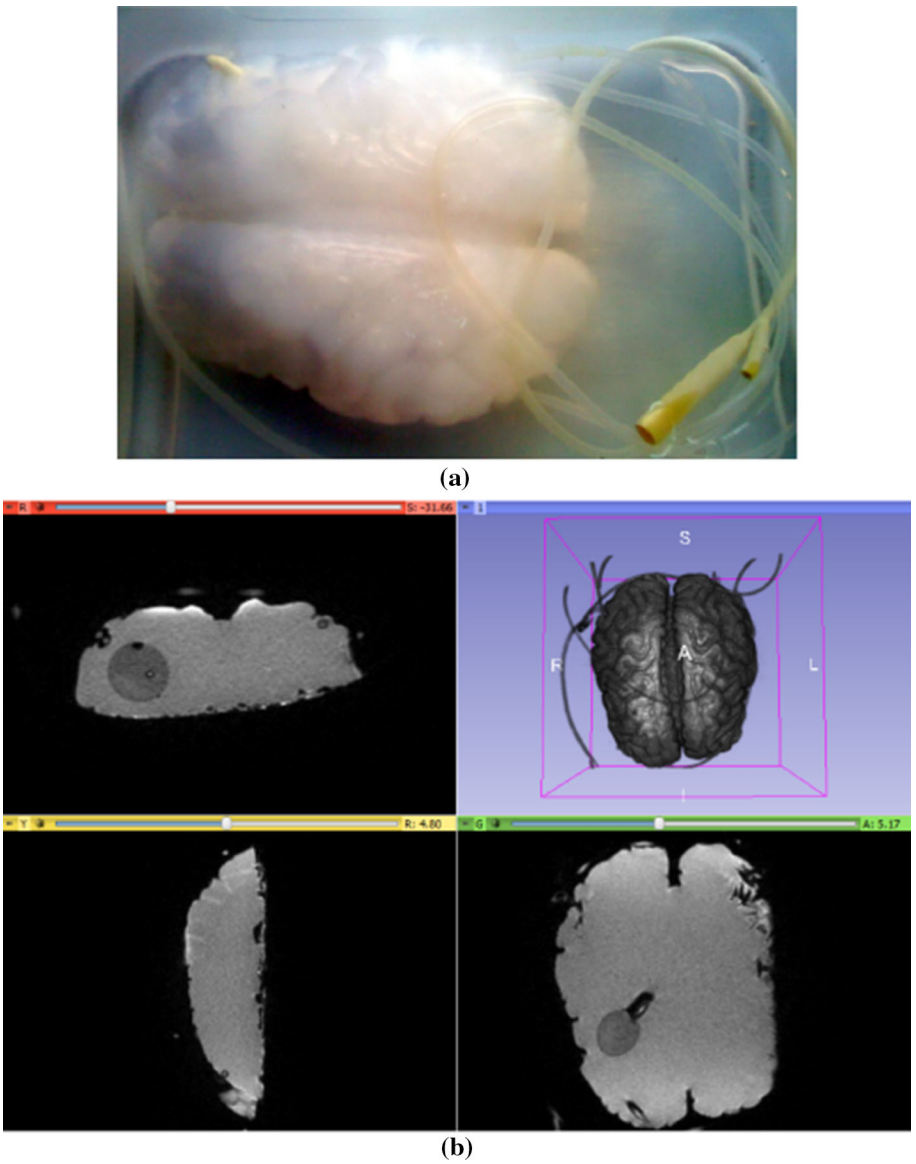

Fig. 2 **a** A picture of brain phantom and **b** the MR image of it when the internal balloon inflated 5 ml, depicted in 3D Slicer software

Initializing FE linear elastic model

Before building the FE model, the brain image was subjected to segmentation. The segmentation of the brain affects the accuracy of mesh generation and surface tracking. The images were segmented using the 3D Slicer [22] software. In the case of the phantom, the inflated balloon was easily segmented. For the animal brain using a reference database of animal anatomy, the major parts such as skull, parenchyma, ventricles, and injected cyst were carefully segmented.

Smoothing segmented regions facilitates the generation a fine volumetric mesh. Using the meshing software IsoSurf [23] and GMesh [24], the phantom and animal brain were meshed to 7152 and 3718 tetrahedral elements, respectively. Figure 4 shows a representative picture of the meshing results.

The number of nodes and elements were usually much less than the number of 3D image voxels. When we created more elements in a certain volume, the computations rapidly increased in a nonlinear manner, whereas the final precision slightly changed. FEM-based studies [16,18] have shown that a total of 15,000 elements were created to reconstruct an entire human brain. It is therefore reasonable that a total of 3718 elements were sufficient to create our animal model, which presented a much smaller brain volume (approximately1/8).

When the deformation was is less than 10 %, FEM can be assumed to follow the linear elastic model (LEM) [16]. This assumption has also been determined to be true in the present study. For the biomechanical parameters of the model, various values for Young's modules can be found in the literature. Based on previous works [16], the parameters

(a)

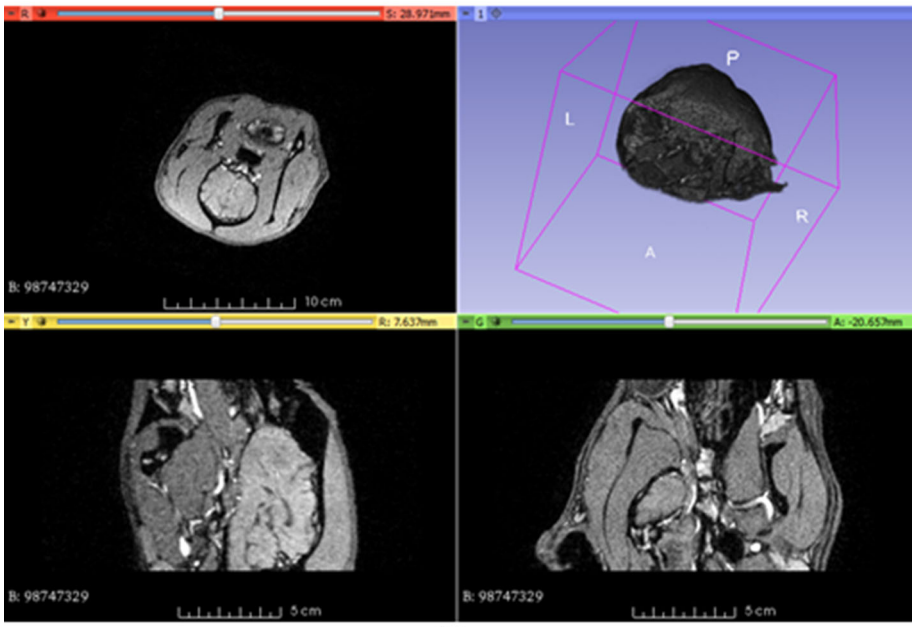

(b)

Fig. 3 **a** The dog under operation and **b** a sample MR image of its head

$E_{par} = 700Pa$ and $\nu_{par} = 0.42$ were used for parenchyma and $E_{csf} = 15Pa$ and $\nu_{csf} = 0.05$ for CSF. Due to its circulation within ventricles, the CSF was modeled as a compressible medium. The fluid inside the balloon in the phantom or simulated cyst in the animal brain was incompressible; therefore, we assessed the physical parameters of the proximal parenchymal tissue.

Capturing surface data

The method used for scanning the surface was based on a simple concept. A checkerboard pattern was projected to the visible surface of the region of interest, and cross points of the projected pattern (referred to as P-land hereafter) were scanned by a stereo camera to calculate their 3D positions. The stereo camera detects the cross points by processing the images that were acquired by two sensors (left and right) and recognizing the visual patterns that match the descriptors in a marker template database. As shown in Fig. 5, it triangulates the two projection lines associated with two image centers to obtain the 3D position of desired point.

The minimum distance of P-lands was limited by the accuracy of camera. A more dense point cloud was thus acquired by sweeping a projected pattern on the surface. The camera that was used in the present study was the Micron Tracker of Claron, Inc., under Parsiss Image-Guided Navigation[1], and the software developed in the previous studies conducted by

[1] Parseh Intelligent Surgical Systems Parsiss Company, Tehran, Iran. www.parsiss.com.

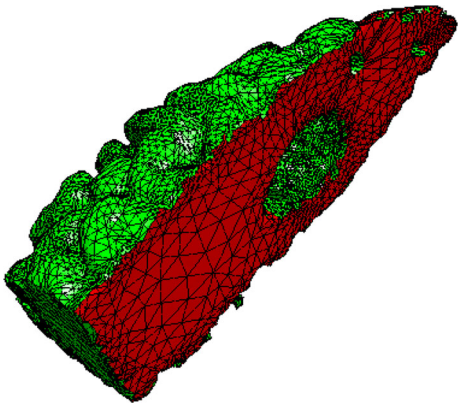

Fig. 4 The meshed subvolume of phantom. The bores are inflated balloon and tubes inside it

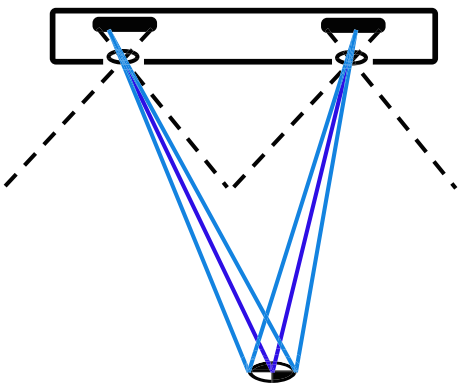

Fig. 5 The concept of triangulation for 3D position calculation

our group [1,20] were used to filter the outliers and duplicated points.

Extracting vascular tree from MRA and doppler US data

The preoperative MRA that was used for extracting the vascular tree was a 3DTOF MRA that featured good contrast quality. A gray level thresholding technique was applied to these images in three steps. A threshold that generates the maximum number of vessels that becomes visible was manually adjusted, and the centerlines of vessels were selected. Outliers were filtered by a proximity measure that discards isolated segmented centerlines. Finally, for the consistency of the results, the vascular tree was visually examined.

For constructing a Doppler US pseudo-volume, we gathered a set of 2D Doppler US images that were localized by the stereo camera during data acquisition. A marker was attached to the US probe, and its 3D position was calibrated before starting surgery. In each 2D image, after isolating colored pixels from B-mode background, some connected pixels or stains corresponding to vessels remained. Some artifacts due to fast freehand motions of the probe were filtered. These

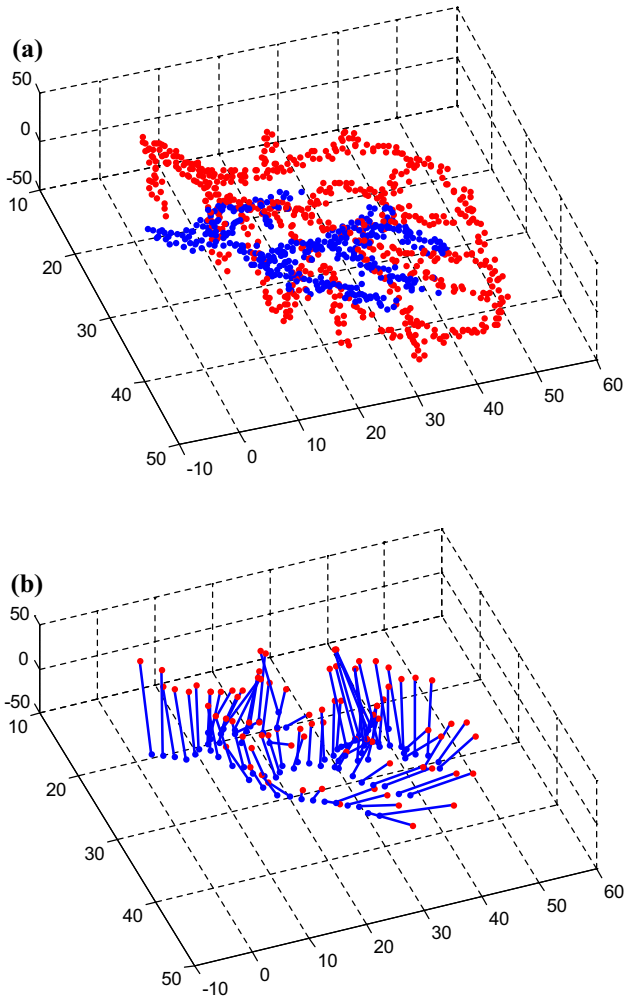

Fig. 6 **a** Point cloud of vessels extracted from MRA (*red*) and Doppler US (*blue*), **b** sparse displacement vectors of vascular tree

usually have a larger area, and thus, we discarded these by a threshold of 8 mm^2. Another problem was the heartbeat that makes small vessels visible in one slice and invisible in the next adjacent slice in space and time. In our animal model, only a few stable centerlines of larger vessels were segmented.

Figure 6 shows the two point clouds that corresponded to the extracted vessels from the MRA and Doppler data and the displacement vectors obtained after their registration.

Non-rigid registration method

Registration of preoperative images to intraoperative ones was at the center of any brain shift estimation approach. In the present study, we required a point matching method to find the nodal displacements in the FE model. We thus developed a non-rigid point matching algorithm that was more compatible with the underlying nature of the deformed object. Among the existing methods, the probabilistic ones such as TPS

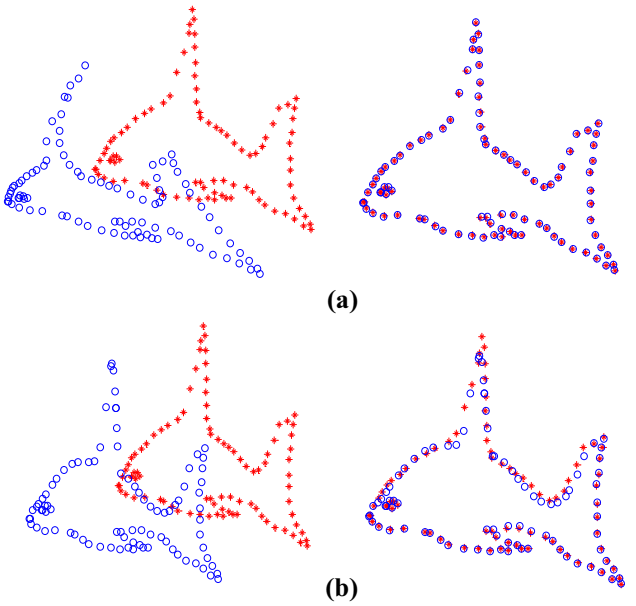

Fig. 7 **a** Myronenko's (the CPD author) example of coherent deformation; All points matched exactly, **b** same example with a non-coherent deformation generated by moving the top of object; points in the top region were not matched exactly

robust point matching (TPS-RPM) [25] and coherent point drift (CPD) [26] have shown better performance, although the deformation method in these algorithms was based only on a mathematical model in which its parameters were obtained from image features. The CPD algorithm showed a generally better performance, although we observed that in some cases, when the assumption of coherent movement was violated, some errors were encountered. Figure 7 shows the famous 2D fish example where CPD showed some deficiency.

This section will describe our findings that a biomechanical model performs better for elastic objects. In our approach, we followed the framework proposed by CPD authors, with some modifications.

CPD review

In the CPD algorithm, the alignment of two point sets was considered as a probability density estimation problem, where one point set represents the GMM centroids and the other one as the data points. The maximum of GMM posterior probability is obtained when two point sets matched. The following notations were employed:

- D : the dimension of point set (2 or 3)
- $\mathbf{x}_1, \ldots, \mathbf{x}_N$: points in first point set (data points)
- $\mathbf{y}_1, \ldots, \mathbf{y}_M$: points in second point set (GMM centroids)
- $\mathbf{T}(\mathbf{y}_m, \theta)$: transform T applied to $\mathbf{y}_m$, where θ is the set of transformation parameters

The GMM probability density function is

$$p\left(\mathbf{x}\right) = \omega\frac{1}{N} + \left(1-\omega\right)\sum_{m=1}^{M} P\left(m\right) p\left(\mathbf{x}|m\right) \tag{1}$$

where $p\left(\mathbf{x}|m\right) = \frac{1}{\left(2\pi\sigma^2\right)^{D/2}} \mathrm{e}^{-\frac{\|\mathbf{x}-\mathbf{y}_m^2\|}{2\sigma^2}}$ and $P\left(m\right) = \frac{1}{M}$. The first term is a uniform distribution is added to mixture model (for $m = M+1$) to account for noise and outliers ($0 \leq \omega \leq 1$).

Using the expectation maximization (EM) algorithm in a Bayesian framework, at the E step, we computed the posteriori probability distributions $P^{\text{old}}(m|\mathbf{x})$ of the mixture components, and at the M step, we estimated θ by minimizing the negative log-likelihood:

$$\begin{aligned} &Q\left(\theta, \sigma^2\right) \\ &= -\sum_{n=1}^{N}\sum_{m=1}^{M+1} P^{\text{old}}\left(m|\mathbf{x}_n\right) \log\left(P^{\text{new}}\left(m\right) P^{\text{new}}\left(\mathbf{x}_n|m\right)\right) \\ &= \frac{1}{2\sigma^2}\sum_{n=1}^{N}\sum_{m=1}^{M} P^{\text{old}}\left(m|\mathbf{x}_n\right) \|\mathbf{x}_n - T\left(\mathbf{y}_m, \theta\right)\|^2 \\ &\quad + \frac{\mathrm{N_p D}}{2} \log\sigma^2 \end{aligned} \tag{2}$$

where $N_p = \sum_{n=1}^{N}\sum_{m=1}^{M} P^{\text{old}}\left(m|\mathbf{x}_n\right) \leq N$, and

$$P^{\text{old}}\left(m|\mathbf{x}_n\right) = \frac{\mathrm{e}^{-\frac{1}{2}\left\|\frac{\mathbf{x}_n - \mathrm{T}\left(\mathbf{y}_m, \theta^{\text{old}}\right)}{\sigma^{\text{old}}}\right\|^2}}{\sum_{k=1}^{M}\mathrm{e}^{-\frac{1}{2}\left\|\frac{\mathbf{x}_n - \mathrm{T}\left(\mathbf{y}_k, \theta^{\text{old}}\right)}{\sigma^{\text{old}}}\right\|^2} + \mathrm{c}} \tag{3}$$

where $\mathrm{c} = \left(2\pi\sigma^2\right)^{D/2}\frac{\omega M}{(1-\omega)N}$.

In the non-rigid CPD method, the transformation of $\mathbf{y}_m$ points was defined as follows:

$$T\left(Y, v\right) = Y + v\left(Y\right) \tag{4}$$

where Y is the matrix of all $\mathbf{y}_m$ points, and $v(Y)$ is a smooth function that drifts $\mathbf{y}_m$ points toward the $\mathbf{x}_n$ points. The coherent motion transformation in CPD algorithm is as follows:

$$T\left(Y, v\right) = Y + GW \tag{5}$$

where G is a predefined Gaussian kernel matrix, and W is the matrix of coefficients. We hereby propose a new smooth function to replace the GW term in the above equation based on the biomechanical features of a deformed object to more accurately match the points in the deformed areas.

New FED method

For a LEM, a linear equation:

$$F = KU \tag{6}$$

relates the vector of external forces F to the vector of displacements U, where K is the stiffness matrix. In this equation, the displacements of nodes were assumed to be small, and we want to use this assumption to write a smooth function for movement of the $\mathbf{y}_m$ points toward the $\mathbf{x}_n$ points. If $\mathbf{y}_m$ points were considered as the nodes of a LEM, a small movement ($U = \Delta Y$) would therefore be:

$$\Delta Y = K^{-1} F \tag{7}$$

where $Y_{MD\times 1} = \left[\mathbf{y}_1^T, \ldots, \mathbf{y}_M^T\right]^T$ is a column vector with $M \times D$ elements. Proper constraints on the LEM should be applied to generate a non-singular K matrix. This can be achieved when the number of supports or fixed nodes in the model is greater than those of moving nodes. The authors of the CPD algorithm also added a regularization term to the likelihood function to enforce the smoothness of displacements, although we claim that the proper K matrix would ensure smoothness of movements. Therefore, the transformation would be as follows:

$$T\left(\mathbf{y}_m, \theta\right) = \mathbf{y}_m + K_m^{-1} F \tag{8}$$

where K_m^{-1} is a $D \times MD$ matrix of rows of K^{-1} corresponding to $\mathbf{y}_m$. Substituting (8) in (2), the F vector, which minimizes the negative log-likelihood, should satisfy the following equation:

$$\sum_{n=1}^{N}\sum_{m=1}^{M} P^{\text{old}}\left(m|\mathbf{x}_n\right) K_m^{-1T}\left(\mathbf{x}_n - \mathbf{y}_m - K_m^{-1} F\right) = 0 \tag{9}$$

After computing for F, the best σ^2 can be obtained by equating the corresponding derivative of Q to zero:

$$\sigma^2 = \frac{1}{N_p D}\sum_{n=1}^{N}\sum_{m=1}^{M}\left\|\mathbf{x}_n - \mathbf{y}_m - K_m^{-1} F\right\|^2 \tag{10}$$

Equations (9) and (10) are the M-step of the EM algorithm. We named this new non-rigid algorithm as the FED and implemented this in the MATLAB software.

We tested some 2D and 3D point sets to compare the performance of FED against CPD. Local deformations were applied by displacing some neighbor points in a local area of the point sets.

Before running FED, some nodes were fixed as support nodes of the LEM such that stiffness matrix becomes non-singular. First, we started the CPD algorithm to align two point sets. After some iteration, the points in the non-deformed area were matched. We used these as the fixed nodes and defined the K matrix element by element to initialize the FED algorithm. Then, CPD was continued, and FED was started to match the same point sets.

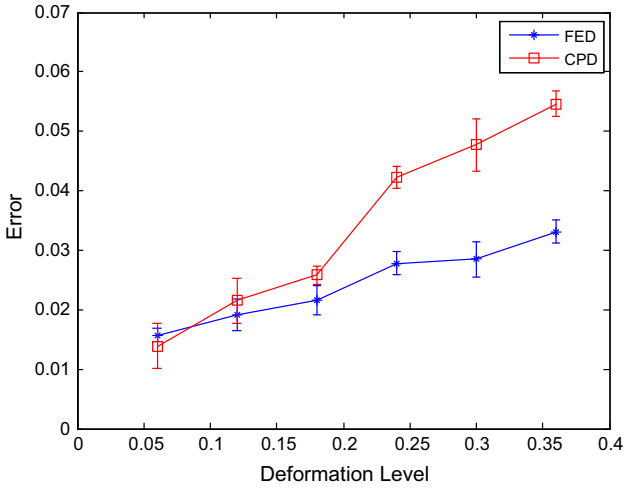

Fig. 8 Registration error for the FED and CPD algorithms when a local deformation in about 10 % of object is applied

Results

FED performance analysis

We tested all point sets provided and used by the CPD authors. Figure 8 shows the registration errors obtained for the CPD and our proposed FED algorithms.

The deformation level in this figure denotes the amount of mean applied displacement. In all cases, the area in which the deformation was applied was approximately 10 % of whole object. Similar to the settings described in the CPD paper, the two point sets were normalized to zero mean and unit variance before registration. Therefore, the units were removed from axis.

As shown in Fig. 8, when the amount of deformation was small, CPD performs slightly better, but when the deformation was larger in the same area, FED outperformed it.

Phantom study

Mean errors that were calculated for the registration tasks in the phantom study are shown in Table 1. Registration errors for the target points are the measure of accuracies obtained for the shift estimation.

Figure 9 shows the box plot of results that are shown in Table 1. These results indicate that when the deformation

Table 1 Registration errors obtained for the surface and target points in two inflation cases of the ballon inside the phantom, 5 and 10 ml

Test no.	Mean error for surface points (mm)		Mean error for target points after FE analysis (mm)	
	5 ml	10 ml	5 ml	10 ml
1	0.48	0.61	1.27	1.41
2	0.66	0.90	1.44	1.63
3	0.83	1.06	1.70	1.92
4	0.39	0.54	0.84	1.03
5	0.54	0.68	1.31	1.18
Average	0.58 ± 0.17	0.76 ± 0.22	1.31 ± 0.31	1.43 ± 0.36

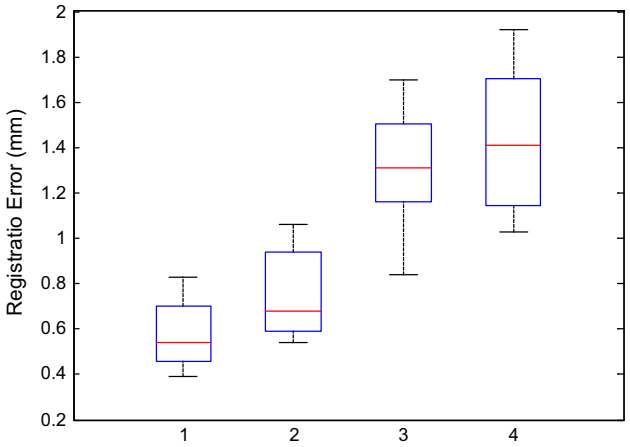

Fig. 9 Registration error for the surface points (1 for 5ml and 2 for 10 ml inflation) and target points (3 for 5 ml and 4 for 10 ml inflation)

increased due to the inflation, the registration errors for surface and target slightly increased.

Animal model study

Registrations were performed by three non-rigid registration methods, namely, TPS-RPM [24], CPD [25], and our proposed FED. Table 2 shows the mean errors for the registration of surface and vascular points. It also shows TREs that were computed after FE analysis using the surface data only, the vessels data only, and finally, a combination of these methods.

The FED method clearly outperformed the other two well-known methods. The results also showed that the accuracy of registration affected the final error that was obtained for the target points after the FE analysis.

The best registration error for the target points reached 1.55 mm using the FED algorithm. The results of combination method were clearly less than those obtained by applying surface and vessels only data. These findings proved the efficiency of our proposed idea of combining the two imaging modalities in reducing the final registration error, thus significantly improving brain shift estimation.

Discussion

In each step of the present study, we encountered several challenging problems. Some of these problems in working with phantom were already observed and resolved in previous studies that were conducted by the authors of the present report [1,21]. In this phantom study, the main difficulties were related to the acquisition of surface data. Adjusting ambient light and the reflections of light from the surface were two important factors that affected the resolution of the surface scan. In addition, these issues also rendered the initial set up to be time consuming. However, several P-lands that were captured by the 3D camera were treated as outliers and should be deleted. Therefore, to acquire more reliable data, the overall procedure can take more time than usual. The main advantages of this method its cost-effectiveness and the absence of contact.

The animal model study encountered more difficulties, especially in the Doppler US data acquisition and processing. Besides the natural problems of Doppler US imaging such

Table 2 Mean registration errors (mm) obtained in animal model study

	Surface points	Vascular points	Target points after FE analysis using		
			Surface data	Vassels data	Combination
FED	1.03	1.91	1.87	2.67	**1.55**
CPD	1.14	2.07	2.11	2.85	1.83
RPM	1.48	2.65	2.36	3.53	2.11

Bold value indicates the best registration error for the target points using the FED algorithm

as noise, the insufficient number of vessels around the tumor region can reduce the useful inputs for the biomechanical model. In fact, for deeper tumors, the deformation was small, and for tumors near the surface, the number of adequately large vessels recoverable in Doppler images was small. Pressure applied on the US probe during data acquisition can also affect the nature of deformation and therefore create CSF movement artifacts. In addition, the rapid movement of the probe can also produce artifacts on the Doppler image.

Also, in the field of registration tasks in the present study, the FED algorithm showed some limitations, which included initial conditioning requirements. Proper definition of stiffness matrix and fixed nodes is a critical step that affects the stability and performance of FED.

One of the questions that the reader of this paper may ask us is why did we use LEM concept in the FED algorithm to drift source points toward target points and then again use the calculated displacement in a FE model to compute deformation. This seems to be a flaw in the design of the study. In fact, in the FED algorithm, we assumed that deformation was local, and the algorithm was initialized by fixing some points around the deformed area, but in the FE analysis, approximately all of the nodes in the volume were included in the computations. In FED, we matched local deformed areas (surface and vessels), but the final FE analysis combined the calculated displacements to compute the deformation of the entire brain.

For surface data acquisition, FED algorithm initialization and image registration can be performed reasonably fast, possibly within a couple of minutes. It is obvious that rendering of 3D Doppler US images and FE analysis were generally time-consuming tasks, but these can be improved using optimized algorithms. As compared to the conventional method of performing intraoperative MR imaging during operating time [27], which is very time-consuming, this method can be of great interest for neurosurgeons, particularly in terms of reducing surgery time.

Conclusions

In the present study, we tried to improve the accuracy of brain shift estimation using a novel approach of combining two intraoperative imaging modalities, namely, surface scanning and Doppler US imaging, in a biomechanical model. A new surface imaging method, projected landmark scanning, and a new non-rigid registration algorithm, FED, were proposed in this work. Validation tests on a phantom and animal model were conducted, and after extensive processing, the results were evaluated.

The results of the present study proved the accuracy and the effectiveness of our method. Although each imaging modality showed some degree of error reduction in brain shift estimation, the proposed combination method has shown an acceptable estimation accuracy approximately 1.55 mm.

Another product of the present study is the proposed biomechanically based FED registration algorithm that can be useful for similar works on elastically deformed objects.

Although one pre-clinical test on animal model is insufficient to fully validate the findings of the present study, it appears that the method of hybrid imaging is a promising technique to generate more accurate results for brain shift compensation in future neuro-navigation systems.

Acknowledgments This Project was supported by the Research Center for Biomedical Technology and Robotics (RCBTR), and Rajaei Cardiovascular, Medical and Research Center, and Parseh Intelligent Surgical Systems (Parsiss Company), Tehran, Iran.

Conflict of interest Amrollah Mohammadi, Alireza Ahmadian, Amir Drabandi Azar, Ahmad Darban Sheykh, Faramarz Amiri and Javad Alirezaie declare that they have no conflict of interest.

Ethical standard All institutional and national guidelines for the care and use of laboratory animals were followed.

References

1. Ahmadian A, Dadashi Serej N, Karimifard S, Farnia P (2013) An efficient method for estimation of soft tissue deformation based on intra-operative stereo image features and point-based registration. Int J Imaging Syst Technol 23(4):294–303. doi:10.1002/ima.22064
2. Nimsky C, Ganslandt O, Cerny S, Hastreiter P, Greiner G, Fahlbusch R (2000) Quantification of, visualization of, and compensation for brain shift using intraoperative magnetic resonance imaging. Neurosurgery 47(5):1070–1080
3. Nabavi A, Black P, Gering D, Westin C, Mehta V, Pergolizz R Jr, Ferrant M, Warfield S, Hata N, Schwartz R, Wells W, Kikinis R, Jolesz F (2001) Serial intraoperative magnetic resonance imaging of brain shift. Neurosurgery 48(4):787–797
4. Reinges M, Nguyen H, Krings T, Hutter B, Rohde V, Gilsbach J (2004) Course of brain shift during microsurgical resection of supratentorial cerebral lesions: limits of conventional neuronavigation. Acta Neurochir 146(4):369–377
5. Trantakis C, Tittgemeyer M, Schneider J, Lindner D, Winkler D, Strauss G, Meixensberger J (2003) Investigation of time-dependency of intracranial brain shift and its relation to the extent of tumor removal using intra-operative MRI. Neurol Res 25(1):9–12
6. Soza G, Hastreiter P, Vega F, Rezk-Salama C, Bauer M, Nimsky C, Greiner G (2003) Non-linear intraoperative correction of brain shift with 1.5 T data. Bildverarbeitung für die Medizin. Springer, Berlin. doi:10.1007/978-3-642-18993-7_5
7. Clatz O, Delingette H, Talos I, Golby A, Kikinis R, Jolesz F, Ayache N, Warfield S (2005) Robust non-rigid registration to capture brain shift from intra-operative MRI. IEEE Trans Med Imaging 24(11):1417–1427
8. Hu J, Jin X, Lee J, Zhang L, Chaudhary V, Guthikonda M, Yang K, King A (2007) Intraoperative brain shift prediction using a 3D inhomogeneous patient specific finite element model. J Neurosurg 106:164–169
9. Hata N, Nabavi A, Wells W III, Warfield S, Kikinis R, Black P, Jolesz F (2000) Three-dimensional optical flow method for mea-

surement of volumetric brain deformation from intraoperative MR images. J Comput Assist Tomogr 24(4):531–538
10. Shattuck D, Leahy R (2002) Brain suite: an automated cortical surface identification tool. Med Image Anal 6(2):129–142
11. Ferrant M, Nabavi A, Macq B, Black P, Jolesz F, Kikinis R, Warfield S (2002) Serial registration of intraoperative MR images of the brain. Med Image Anal 6(4):337–359
12. Kyriacou S, Davatzikos C, Zinreich S, Bryan R (1999) Nonlinear elastic registration of brain images with tumor pathology using a biomechanical model. IEEE Trans Med Imaging 18(7):580–592
13. Miga M, Sinha T, Cash D, Galloway R, Weil R (2003) Cortical surface registration for image-guided neurosurgery using laser-range scanning. IEEE Trans Med Imaging 22(8):973–985
14. Comeau R, Sadikot A, Fenster A, Peters T (2000) Intraoperative ultrasound for guidance and tissue shift correction in image-guided neurosurgery. Med Phys 27:787–800
15. Reinertsen I, Lindseth F, Unsqaard G, Collins D (2007) Clinical validation of vessel-based registration for correction of brain-shift. Med Image Anal 11(6):673–684
16. Bucki M, Palombi O, Bailet M, Payan Y (2012) Doppler ultrasound driven biomedical model of the brain for intraoperative brain-shift compensation: a proof of concept in clinical conditions. In: Payan Y (ed) Soft tissue biomechanical modeling for computer assisted surgery. Studies in mechanobiology, tissue engineering and biomaterials series, vol 11. Springer, pp 135–165. doi:10.1007/978-3-642-29014-5
17. Hjelmeland A, Lathia J, Sathornsumetee S, Rich J (2011) Twisted tango: brain tumor neurovascular interactions. Nat Neurosci 14(11):1375–1381
18. Joldes G, Wittek A, Couton M, Warfield S, Miller K (2009) Real-time prediction of brain shift using nonlinear finite element algorithms. In: Yang G, Hawkes D, Rueckert D, Noble A, Taylor C (eds) Medical image computing and computer-assisted intervention (MICCAI 2009). Lecture notes in computer science, vol 5762. pp 300–307. doi:10.1007/978-3-642-04271-3_37
19. Mendoza C, Laugier C (2003) Tissue Cutting using finite elements and force feedback. In: Ayache N, Delingette H (eds) Surgery simulation and soft tissue modeling. Lecture notes in computer science, vol 2673, pp 175–182. doi:10.1007/3-540-45015-7_17
20. Dadashi Serej N, Ahmadian A, Mohagheghi S, Sadrehosseini SM (2014) A projected landmark method for reduction of registration error in image-guided surgery systems. Int J Comput Assist Radiol Surg 10(5):541–554. doi:10.1007/s11548-014-1075-z
21. Farnia P, Ahmadian A, Khoshnevisan A, Jaberzadeh A, Dadashi Serej N, Kazerooni AF (2011) An efficient point based registration of intra-operative ultrasound images with MR images for computation of brain shift; A phantom study. Proceedings of IEEE conference on engineering in medicine and biology (EMBS 2011) pp 8074–8077. doi:10.1109/IEMBS.2011.6091991
22. Free and open source software package for visualization and medical image computing. Brigham and Women's Hospital, Harvard Medical School. http://www.slicer.org/
23. Free software for extracting triangulated iso-surfaces from a block of data. Machine Intelligence Laboratory, Department of Engineering, Cambridge University. http://mi.eng.cam.ac.uk/~gmt11/software/isosurf/isosurf.html
24. Free software for 3D finite element grid generation. Dept. of Electrical Engineering and Computer Science, University of Liege. http://www.geuz.org/gmsh/
25. Chui H, Rangarajan A (2003) A new point matching algorithm for non-rigid registration. Comput Vis Image Underst 89(2/3):114–141
26. Myronenko A, Song X (2010) Point set registration: coherent point drift. IEEE Trans Pattern Anal Machine Intell 32(12):2262–2275
27. Lewin JS, Nour SG, Meyers ML, Metzger AK, Maciunas RJ, Wendt M, Duerk JL, Oppelt A, Selman WR (2007) Intraoperative MRI with a rotating, tiltable surgical table: a time use study and clinical results in 122 patients. AJR Am J Roentgenol 189(5):1096–1103. doi:10.2214/AJR.06.1247